Separating Intrinsic and Extrinsic Responses of Whisker Sensors Using Accelerometer

Prasanna K. Routray, *Member, IEEE*, Debadutta Subudhi, *Student Member, IEEE*, Basak Sakcak, *Member, IEEE*, Steven M. LaValle, *Senior Member, IEEE*, Pauline Pounds, *Member, IEEE*, and M. Manivannan, *Member, IEEE*

***Abstract*—Rodents and Felidae whiskers are highly sensitive, detecting extrinsic inputs such as airflow or contact and intrinsic inputs such as base vibrations or self-induced motion. Building effective artificial whisker sensors faces a challenge due to the intricate coupling of responses at the whisker base. There is a research gap in understanding whisker sensors' responses to intrinsic and extrinsic inputs. To address this, we propose two methods, using base acceleration as a reference input: 1) employing frequency-domain adaptive filtering (FDAF) and 2) introducing the base vibration response model (BVRM) that mathematically represents the whisker sensor's behavior to base vibrations or self-induced motion. Validation of FDAF and BVRM is conducted through simulation and experimentation. The BVRM excels in both simulation and experiment, demonstrating a signal-to-noise ratio (SNR) of 35.20, slightly outperforming the laboriously tuned partitioned constrained FDAF with an SNR of 34.96, despite FDAFs slower convergence and poorer performance in experiments. In addition, BVRM can be useful in filtering sensor responses for independent use cases, such as terrain identification, flow sensing, and surface profile identification. By separating responses to extrinsic and intrinsic inputs without discarding either, whisker sensors become more versatile and multipurpose.**

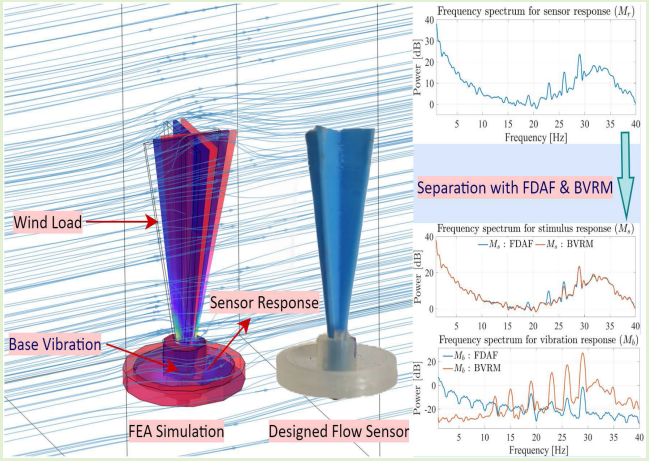

***Index Terms*— Fluid flow sensing, system identification, tactile sensing, vibration isolation, whisker sensor.**

I. Introduction

WHISKER sensors offer highly sensitive tactile and fluid flow sensing for mobile robots at low cost. However, their sensitivity to motion means that they also capture vibrations from their mounting platforms. Differentiating between external inputs and internal vibrations from the robot or self-induced motion is challenging due to the robot's mechanical dynamics. Whiskers, which act like cantilever beams, are affected by both types of inputs, leading to structural changes based on their shape, size, and material composition [1], [2].

Rodents and Felidae use whiskers for environmental exploration, prey detection, and surface interaction [3]. Inspired by these sensory capabilities, researchers have replicated and studied whiskers' characteristics and mechanisms [4]. Mobile robots adopt whiskers to understand their surroundings with minimal electronic interference [5], measuring several parameters at the base, including bending moment [6]. Acting like cantilever beams, these sensors measure moments upon contact along the longitudinal axis. Whisker sensor technology dates back to 1984 when Russell created a binary whisker sensor array to detect objects in unstructured environments [5]. Later, the WhiskerBOT [7] advanced the understanding of rat whisker mechanics and neuroscience. Russell's subsequent work focused on object shape recognition for robotic manipulation [8]. Recent developments in fluid flow sensing include Hall effect-based designs for identifying wind

Received 13 August 2024; accepted 26 August 2024. Date of publication 16 September 2024; date of current version 31 October 2024. The associate editor coordinating the review of this article and approving it for publication was Prof. Mohammed Jalal Ahamed. *(Corresponding author: Prasanna K. Routray.)*

Prasanna K. Routray, Debadutta Subudhi, and M. Manivannan are with the Touch Laboratory, Center for Virtual Reality and Haptics, Indian Institute of Technology Madras, Chennai 600036, India (e-mail: prasanna.routray97@gmail.com; dev.subudhi49@gmail.com; mani@iitm.ac.in).

Basak Sakcak and Steven M. LaValle are with the Center for Ubiquitous Computing, Faculty of Information Technology and Electrical Engineering, University of Oulu, 90570 Oulu, Finland (e-mail: basak.sakcak@oulu.fi; steven.LaValle@oulu.fi).

Pauline Pounds is with the School of Information Technology and Electrical Engineering, The University of Queensland, Brisbane, QLD 4072, Australia (e-mail: pauline.pounds@uq.edu.au).

Digital Object Identifier 10.1109/JSEN.2024.3452206

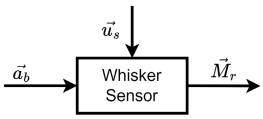

Fig. 1. Whisker sensor sensing scheme: $\vec{a}_b$ represents the intrinsic input (base vibration due to terrains or the robot itself) and $\vec{u}_s$ denotes the extrinsic input (fluid flow) to the whisker sensor. $\vec{M}_r$ is the combined sensor response to both intrinsic and extrinsic inputs.

gusts [9], [10], [11] and capacitive sensors for the same purpose [12], [13], [14], [15]. Optical sensing mechanisms using image processing have also been studied to capture whisker sensor responses [16], [17]. In all these designs, the complex interplay of extrinsic and intrinsic inputs affecting the sensor response is evident.

Whisker sensors on mobile platforms are affected by the platform's motion. Adaptive filtering can reduce the impact of a robot's self-motion on these sensors [18]. They respond to both external stimuli and the robot's dynamics and terrain. Vision-based sensing for detecting contact, airflow, and inertia using multiple whiskers was proposed [17], but distinguishing inertia and stimuli for a single whisker remains unclear. Bayesian methods with a microaerial vehicle model were used to estimate airflow, drag, and stimuli [19]. Platform-independent whisker sensors complicate separating intrinsic and extrinsic responses. Integrating whiskers into robots for terrain identification [20], [21], noncontact sensing [22], and surface profile determination [23], [24] underscores the need to separate these responses, which is the focus of this work. Moreover, whiskers are used in autonomous underwater vehicles (AUVs) inspired by aquatic animals, such as seals and pinnipeds [25], [26]. These animals possess undulated, wavy-structured whiskers that help reduce vibrations caused by vortices generated downstream during upward movement. These vortex-induced vibrations are external inputs, similar to the scenario of a static whisker in a moving fluid.

This article is organized as follows. Section II describes the problem statement. Section III details the proposed methods for separating sensor responses to vibration and stimuli, including adaptive filters and a model-based method, along with the mathematical model for base vibration in Section IV. Section V presents the simulation setup, the whisker sensor conceptual design, and the finite element analysis (FEA). The experimental study is discussed in Section VI. Sensor response and model identification are covered in Section VII, followed by results and discussion in Section VIII, and conclusion in Section IX.

II. Problem Formulation

Whisker sensors respond to various inputs, resulting in forces and moments at the base. Fig. 1 illustrates the typical sensor response as the resultant bending moment vector ($\vec{M}_r$), considering it as a multiple-input multiple-output (MIMO) system [27]. $\vec{M}_r$ is the sum of bending moments caused by both the extrinsic input vector ($\vec{u}_s$) and the intrinsic input vector ($\vec{a}_b$) in a deterministic sense. Here, vector $\vec{a}_b$ represents the 3-D intrinsic input, such as base vibration or self-induced motions, while vector $\vec{u}_s$ denotes the extrinsic input, such as contact or noncontact stimuli.

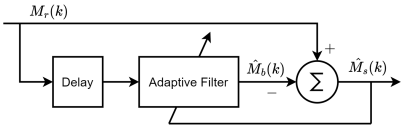

(a) Filter with the notion of delay.

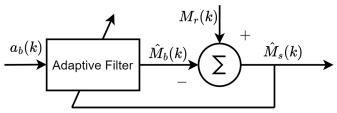

(b) Filter with reference signal.

Fig. 2. Adaptive filters. (a) Separation scheme employing delay and (b) utilization of a correlated reference signal (a_b), where M_b is correlated with a_b. Predicted responses $\hat{M}s$ and $\hat{M}b$ are obtained.

The objective is to decompose the recorded data from a whisker sensor, denoted by $\vec{M}_r$, into two distinct components: $\vec{M}_s$ and $\vec{M}_b$. $\vec{M}_s$ represents the sensor's response to $\vec{u}_s$, while $\vec{M}_b$ represents the response to $\vec{a}_b$. This distinction is necessary for downstream tasks, where the scenario may require a response related to base vibration, stimulus response, or a combination of both. The problem is formally defined by the following equation:

$$\begin{aligned} \vec{M}_r &= \vec{M}_s \oplus \vec{M}_b \\ \vec{M}_s &= f(\vec{u}_s) \\ \vec{M}_b &= g(\vec{a}_b) \end{aligned} \tag{1}$$

where f and g are functions that map $\vec{u}_s$ and $\vec{a}_b$ to $\vec{M}_s$ and $\vec{M}_b$, respectively. These mappings may exhibit linearity within limited input ranges for both $\vec{u}_s$ and $\vec{a}_b$. These equations underscore the challenge of distinguishing between stimulus and base vibration in the whisker sensor system under varying operating conditions, including sensing method (contact or noncontact), sensor structure (resonance modes and damping), and output data rate (ODR).

To the best of the authors' knowledge, there is a gap in the literature addressing the challenge of segregating whisker responses into extrinsic ($\vec{M}_s$) and intrinsic responses ($\vec{M}_b$), despite its significant importance in various applications [20], [22]. This study proposes two unique filtering techniques: 1) an adaptive filter-based technique and 2) a base-vibration response model (BVRM)-based technique, both using an accelerometer as a reference to estimate $\vec{M}_b$ and $\vec{M}_s$. The study highlights the diminishing efficacy of adaptive filters across a broad frequency spectrum, under noisy accelerometer reference and nonuniform coherency in signals of interest. In response to this limitation, a model-based method BVRM, which can be linear or nonlinear, emerges as a better option than the adaptive filter. Physics-based simulations and the development of a basic mathematical model for the whisker BVRM support these findings. The linear time-invariant (LTI) BVRM demonstrates good estimation of M_b and M_s in FEA-based simulations and performs fairly well in experimental setups.

III. Proposed Approach

After discussing the problem, we devise strategies to separate the sensor response M_r in 1-D. While some whisker

sensor designs are curved, as in [28], most whisker-inspired sensor designs are symmetric and cylindrical. Therefore, we consider the symmetric nature of the whisker design and proceed with 1-D analysis.

Popular adaptive filters are considered for separating the sensor response M_r, which is examined first. Notably, both extrinsic and intrinsic inputs are nonstationary. The adaptability and time-varying nature of adaptive filters make them appealing. They demonstrate suitability not only for impulse inputs but also for Gaussian inputs. However, challenges arise in terms of convergence and complexity [29]. The intricacies stem from selecting a specific adaptive filter algorithm and the time required for convergence. Time complexity becomes pivotal, particularly when dealing with highly dynamic inputs in addition to the dynamic and nonadditive nature of intrinsic inputs [30]. In light of these considerations, an adaptive filtering technique based on the Wiener filter [31] emerges as a promising strategy tailored to address this specific problem.

Model-based estimation of M_b and M_s is another commonly used strategy in vibration suppression techniques, such as in atomic force microscopes (AFM) [32] or with piezoactuators [33]. This approach is also applied for isolating or compensating vibrations in AFMs. In the subsequent subsections, we delve into discussion on both adaptive and model-based methods suitable for estimating M_s and M_b without requiring a model of the vehicle on which the whisker is mounted.

A. Adaptive Filters

The interference cancellation method based on the Wiener filter aims to minimize the mean-squared error (MSE) between the measured sensor response $[M_r(k) = M_s(k) + M_b(k)]$ and the estimated signal $\hat{M}_b(k)$ in discrete-time form [29]. The underlying assumption is that the Wiener filter's estimated signal $\hat{M}_b(k)$, also termed as estimated interference, is a linear combination of $a_b(k)$ and is correlated with $M_b(k)$. The reference input $a_b(k)$ depends on whether the base motion is periodic or unpredictable. In field robotics, where movement and terrain are unpredictable, periodic motion is less relevant. If the motion is repetitive, $a_b(k)$ will also be repetitive. However, when the motion is unpredictable, characterizing $a_b(k)$ is challenging, and this is where an accelerometer proves helpful. The fundamental Wiener filter is expressed in (2). The output of this adaptive filter converges to $M_s(k)$ (given $M_b(k) = g(a_b(k))$) as the filter converges over time. Subsequent equations are tailored from the Wiener filter to suit the specific problem addressed in this study

$$\begin{aligned} \text{MSE} &= \mathbb{E}\Big[\big(M_r(k) - \hat{M}_b(k)\big)^2\Big] \\ &= \mathbb{E}\Big[\big(M_r(k) - \mathbf{w}^T a_b(k)\big)^2\Big] \\ \mathbf{w}^* &= \underset{w}{\text{argmin}}\Big(\mathbb{E}\Big[\big(M_r(k) - \mathbf{w}^T a_b(k)\big)^2\Big]\Big) \\ \mathbf{w}^* &= R_{bb}^{-1} r_{bs} \end{aligned} \tag{2}$$

here $R_{bb} = \mathbb{E}[a_b(k)a_b^T(k)]$ represents the autocorrelation matrix, $r_{bs} = \mathbb{E}[M_r(k)a_b(k)]$ is the cross-correlation vector, and $\mathbf{w}$ denotes the time-domain filter weights. The subsequent section outlines the appropriate methods and our approach for estimating M_s and M_b using the adaptive filter.

Depending on the characteristics of the downstream task, an adaptive filter can effectively filter signals under different scenarios. For instance, if the extrinsic input response is narrowband and the intrinsic input response is wideband, employing an adaptive filter is beneficial. Conversely, if the extrinsic input is wideband and the intrinsic input is narrowband, the adaptive filter remains a suitable choice. In addition, the periodic interference from intrinsic inputs can be mitigated by using a delayed response as a reference, as illustrated in Fig. 2(a). Although estimating the delay from the sensor output's frequency response seems practical [29], in real-world applications, information about stimulus and interference periods is often unavailable. This situation necessitates the use of a reference or model-based interference cancellation approach.

When dealing with nonstationary sensor responses that cannot be adequately handled using the previously described delayed adaptive filter method, an alternative approach is necessary. It becomes crucial to introduce a reference signal that correlates well with either the intrinsic or extrinsic input. Fig. 2(b) illustrates an adaptive scheme utilizing such a reference signal. The key assumption here is that $M_b(k)$ and a known reference $a_b(k)$ exhibit a strong correlation. In this scenario, the sensor response $M_r(k) = M_s(k) + M_b(k)$ is composed, where $M_b(k)$ correlates with a measurable reference signal $a_b(k)$. The effective estimation of M_s and M_b hinges significantly on the assumption of high correlation between $M_b(k)$ and the known reference signal $a_b(k)$.

To implement adaptive filters in both the frequency and time domains, discrete-time sensor responses and references collected using a microcontroller unit (MCU) can be utilized for signal separation. The adaptive filter serves as a readily available and valuable tool, particularly when there is a comprehensive understanding of the base vibration. However, the sluggish convergence rate in the least-mean-square (LMS) method and the influence of high-frequency base vibrations may lead to a decline in the performance of adaptive filters. While the normalized-LMS (NLMS) method offers faster convergence, it is accompanied by the drawback of noise amplification.

B. Response Separation With BVRM

Despite the advantages and drawbacks associated with adaptive filters, acquiring a mathematical understanding of the whisker system proves beneficial. This mathematical model also serves as the foundation for implementing model-based signal separation. A system formulated in LTI form shows phase shift near the resonance modes in higher order systems (specifically, second order and above). These phase shifts can cause delays in the system output depending on the system input frequency, necessitating highly precise adaptive filtering, which can be effectively managed by BVRM. The consideration of a system model for signal separation is discussed below.

The model-based vibration control or suppression method, as tested in AFM and piezoactuators using techniques such as model inversion [33] or inverse feed-forward approaches [32], can be adapted for estimating $\hat{M}_s$ and $\hat{M}_b$ using a_b (accelerom-

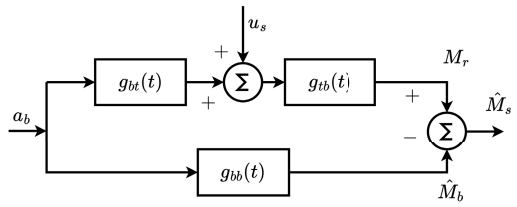

Fig. 3. LTI representation of whisker sensor is depicted alongside BVRM g_{bb}. g_{bt} is the whisker sensor impulse response function (IRF) for input at base and output at base. g_{tb} is the whisker sensor IRF for input at tip and output at tip. g_{bb} is the whisker sensor IRF for input at the base and output at the base. $M_r(k)$ and $M_b(k)$ are approximately equal for an LTI model, where $g_{bb} = g_{bt} \cdot g_{tb}$, given $u_s(t) = 0$. $a_b(t)$ is the base vibration.

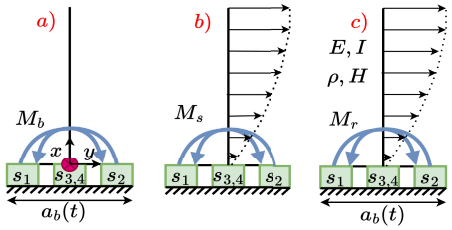

Fig. 4. In the general scenario for whiskers, sensors $s_{1...4}$ at the cantilever base measure the overall bending moment (M_r). Scenarios include (a) sinusoidal base vibration (a_b) induces a moment (M_b). Pay attention to the sensor reference frame (red dot) and (b) fully developed wind load, an extrinsic input, results in a moment (M_s) represented as a parabolic distribution. (c) Combined intrinsic and extrinsic inputs result in the overall moment (M_r). Here, E, I, ρ, and H represent the whisker properties: modulus of elasticity, area moment of inertia, density, and length, respectively.

eter readings). Moreover, this method holds promise for sensorless estimation of M_b, which has potential use in terrain identification or classification if we use BVRM and a_b as input. In addition, it is worth noting that the response from base vibration may be mitigated through the proper mechanical design, a topic beyond the scope of this work but remains a subject of study in the realm of whisker sensors.

In Fig. 3, the model-based approach for estimating $\hat{M}_s$ and $\hat{M}_b$ in an LTI system is illustrated. Referring back to (1), where $\hat{M}_s$ is the predicted sensor response to the stimulus, g_{bb} is the whisker sensor impulse response to the vibration input at the base (where the sensors are located) to measure the output again at the base. A basic comparison between the sensor response (M_r) and the model-predicted sensor response to base vibration $\hat{M}_b$ helps estimate $\hat{M}_s$. In the subsequent section, we introduce a simple mathematical model that emulates the moving platform of a whisker sensor and the resultant moment at the base.

IV. Mathematical BVRM

We adopt a mathematical model that describes the linearized response of a cantilever beam under uniformly varying load (UVL) and sinusoidal base excitation, as outlined in [34]. For sinusoidal base excitation, the sensor response at the base, denoted by M_b, is a function of the base vibration (a_b), where $a_b(t) = a\sin(\omega_b t)$. Here, a represents the amplitude in terms of $g = 9.81, \text{m/s}^2$, ω_b signifies the input frequency to the base of the cantilever in radians, and M_b denotes the moment at the base, as depicted in Fig. 4.

In Fig. 4(a), the input to the whisker system is base vibration in "g," and the output is the moment at the base, which depends on whisker deflection. The governing equation for this deflection due to sinusoidal base vibration [2] along the y-axis is given as follows:

$$\text{EI}\frac{\partial^4 y}{\partial x^4} + \rho\frac{\partial^2 y}{\partial t^2} = -\rho a_b(t) \tag{3}$$

where density (ρ), modulus of elasticity (E), and moment of inertia (I) are the known material properties.

The solution to the governing equation in (3) is of the form

$$y(x,t) = \sum_{n=1}^{N} Y_{b_n}(x)T_n(t) \tag{4}$$

where N is the number of frequency modes, Y_{b_n} is the whisker deflection in y for a given x, and T_n is the temporal change of deflection due to base acceleration in time t. Substituting $y(x,t)$ in (3) and applying the orthogonality of eigenvectors Y_{b_n}, the differential equation simplifies to

$$\frac{d^2}{dt^2}T_n(t) + \frac{\text{EI}\beta_n^4}{\rho}T_n(t) = -a_b\int_0^H \rho Y_{b_n}(x)dx \tag{5}$$

where $\beta_n = -c_n^2(\rho/\text{EI})^{(1/4)}$, c_n is the eigenvalues related to each mode shapes, and H is the height of the beam. The value of β_n is unique for each mode shape of the cantilever beam [2].

The eigenvectors $Y_{b_n}(x)$ are given by

$$Y_{b_n}(x) = \frac{1}{\sqrt{\rho H}}\cosh(\beta_n x) - \cos(\beta_n x) - \frac{\cosh(\beta_n H) + \cos(\beta_n H)}{\sinh(\beta_n H) + \sin(\beta_n H)}.[\sinh(\beta_n x) - \sin(\beta_n x)]. \tag{6}$$

The whisker's structural and environmental damping can be represented by the damping ratio (ζ) in the following equation:

$$\ddot{T}_n(t) + 2\zeta\omega_n\dot{T}_n(t) + \omega_n^2 T_n(t) = -\Gamma_n a_b(t) \tag{7}$$

where $\omega_n^2 = (EI/\rho)\beta_n^2$, and $\Gamma_n = \int_0^H \rho Y_{b_n}(x)dx)$.

Applying the Laplace transform to (7) with zero initial conditions yields the following expression:

$$s^2 T_n(s) + 2\zeta\omega_n s T_n(s) + \omega_n^2 T_n(s) = -\Gamma_n a_b(s). \tag{8}$$

The following presents the transfer function $G(s)$ describing the cantilever's response to the input base vibration

$$G(s) = \frac{T_n(s)}{a_b(s)} = \frac{-\Gamma_n}{s^2 + 2\zeta\omega_n s + \omega_n^2}. \tag{9}$$

The moment at the whisker base M_b sensed by the whisker sensor due to base vibration a_b from (4) results in

$$M_b(x,t) = -EI\frac{d^2 y(x,t)}{dx^2} = -EI\sum_{n=1}^{N}\frac{d^2 Y_{b_n}(x)}{dx^2}T_n(t). \tag{10}$$

The sensor response to fluid flow and the calculation of the flow sensor's area moment of inertia can be found from basic principles. The mathematical model, presented in LTI form for

estimating M_s and M_r, is further analyzed through FEA-based simulation and experiment in subsequent sections.

V. Simulation Setup

The simulation encompasses COMSOL-assisted FEA, the design of a whisker sensor inspired by existing models, and the implementation of base vibration functionality resembling a shaker table. In studies concerning whiskers, the fundamental physics frequently revolves around fluid–structure interaction (FSI), merging principles of structural mechanics with fluid dynamics, encompassing mediums such as air, water, or viscous fluids. This section establishes the foundational elements pivotal to the simulation process.

A. Whisker Sensor

The design of the whisker sensor draws inspiration from the sensor models outlined in [28] and [35], conceptualized as fluid-flow sensor featuring a fin structure, as illustrated in Fig. 5(a). The physical sensor is shown in Fig. 5(b). The material selection for the whisker sensor model is informed by prior literature. Key components of the model comprise the following.

1) *Compliant Element:* A silicone gel with a Shore hardness of 20 A, configurable to achieve desired damping and compliance properties.
2) *Whisker Element:* Nitinol flexible wire ($\Phi = 0.58$ mm).
3) *Fin Element:* Polylactic acid (PLA) is utilized for 3-D printing of the fin element, featuring a density of $\rho = 1230\ \mathrm{kg\,m^{-3}}$, an elasticity modulus of $E = 4.1$ GPa, and a Poisson's ratio of $\nu = 0.35$.
4) *Hall Sensor:* A Hall element is employed to sense the response at the base.
5) *Accelerometer:* Utilized to measure base vibration or motion across three axes.

The characterization of the silicone gel employs the Yeoh model [36]. Model parameters are determined through optimization against experimental stress–strain data, acquired using a microtensile testing machine. The sample specimen used adheres to ASTM D395 standard size specifications [37]. The Yeoh model parameters are $c_1 = 3.4 \times 10^5$ Pa, $c_2 = 1.7152 \times 10^5$ Pa, and $c_3 = 1.32 \times 10^8$ Pa. The bulk modulus is set to $K = 1.5 \times 10^9$ Pa.

B. Vibration Bench

The vibration bench and sensor mounting scheme are shown in Fig. 6(a) similar to the abstract figure where wind and base vibration input is given to the sensor and response at base recorded. A wideband characteristic is essential for the vibration shaker table. Simulation results indicate the first mode of natural frequency is below 50 Hz for whisker and flow sensor. Given a sampling rate of 1 kHz, the input vibration frequency can go up to 500 Hz according to the Nyquist criterion. However, by limiting the input vibration frequency to 200 Hz, we are effectively oversampling, which helps to reduce quantization noise density. Drawing from [38], multisine input signals are designed with

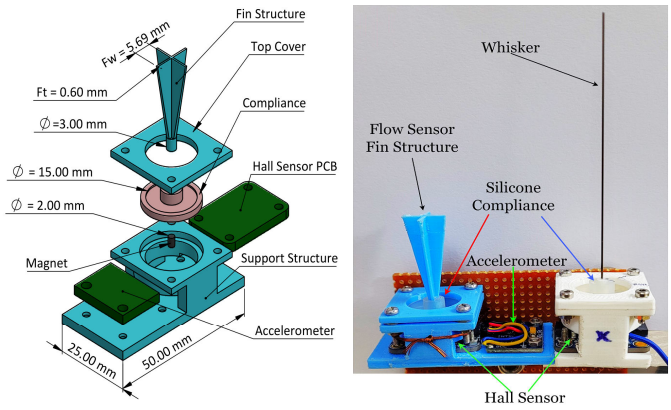

(a) Experimental setup schematic (b) Flow sensor and Whisker sensor

Fig. 5. Whisker-inspired sensor design features both a fin structure for the flow sensor and a cylindrical straight whisker element for the whisker sensor. (a) *CAD design and dimensions:* The sensor's CAD design shows a fin structure for the flow sensor that tapers from top to bottom, made from PLA. Silicone gel is used as a compliant element, allowing the detection of moments resulting from both contact and noncontact interactions. (b) *Physical sensor:* The assembled sensor comprises such as whisker sensor and flow sensor having silicone rubber compliant element, and an accelerometer, all mounted on a PLA support structure.

amplitude $a_b(t)$ and phase ϕ

$$a_b(t) = A \sum_{n=1}^{l} \sin(2\pi f_i t + \phi_i)$$
$$\phi_i = -\frac{i(i-1)\pi}{l}; \quad 2 \le i \le l \tag{11}$$

where l is the total number of frequencies (f_i) and amplitude scaling (A) is chosen according to the experimental input conditions. In this work, the base acceleration input varies in the range of ± 0.01 g to 1.2 g as found in the literature [39].

In COMSOL, multisine signals are utilized to apply volumetric loads to the structure, creating the desired base vibration. These multisine signals are used without reducing the crest factor. For precise measurement of base vibration, a well-calibrated accelerometer is preferred. In addition, transforming sensor measurements to the accelerometer reference frame can be expressed as $M_{rA} = T \cdot M_{rS}$, where M_{rA} and M_{rS} represent the sensor measurements in the accelerometer reference frame and sensor reference frame, respectively.

C. Boundary Conditions

The COMSOL-based FEA simulation setup aims to mimic the experimental arrangement, incorporating base vibration and external stimuli. Base vibration is induced via a volumetric load, resulting in base acceleration, while the external stimulus involves periodic airflow to the whisker sensor. Fig. 6(b) depicts the simulation setup in COMSOL.

In this study, fluid flow pertains to the airflow around the whisker sensor. The fluid inlet boundary condition is prescribed with a velocity of $1\ \mathrm{m\,s^{-1}}$ at 5 Hz, while the outlet remains at static zero pressure. The amplitude of whisker base vibration corresponds to vehicle vibration amplitudes ranging from 0.01 g to 1.3 g. Thus, the boundary condition at the

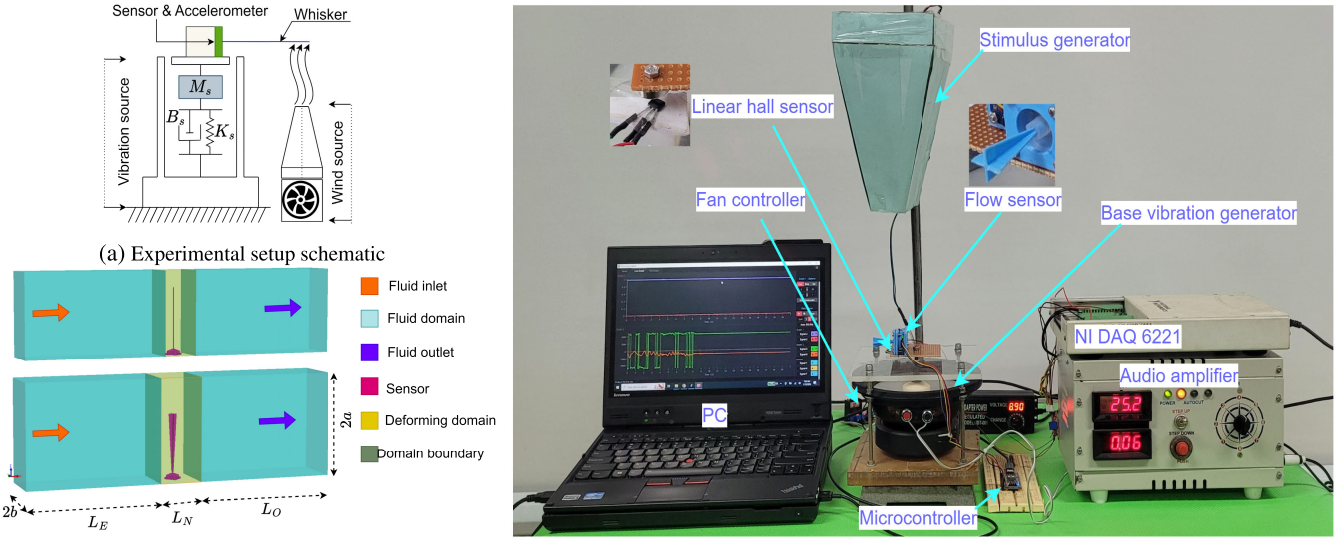

(a) Experimental setup schematic

(b) FEA simulation setup in COMSOL

(c) The experimental setup

Fig. 6. Experimental setup. (a) Schematic of the experimental setup that comprises a whisker-inspired sensor, vibration bench, and stimulus input. (b) FSI study in COMSOL that involves base vibration and airflow for both the whisker sensor (top) and the flow sensor (bottom). The parameters L_E, L_N, and L_O denote the entry, exit, and neck length, respectively, of the fluid domain, with a volume of $(L_E+L_N+L_O)\times 2(a+b)$. (c) The voice-coil (VC) actuator serves as an intrinsic input generator for base vibration, while a controlled CPU fan acts as an extrinsic input generator.

whisker base remains $a_b(t) = A \cdot \sum_{i=1}^{10} \sin(\omega_{bi} t)$ g, where ω_{bi} denotes the base frequencies for time "t" of 1 s. The frequency spectrum for the test signal spans from 1 to 200 Hz.

VI. Experimental Setup

The practical setup, depicted in Fig. 6(c), replicates a mobile robotic platform equipped with a whisker, mirroring the simulated environment described earlier. The system comprises a flow sensor inspired by a whisker, a custom-built VC actuator (96 W), and a high-performance audio amplifier (600 W: class-D amplifier TAS5630 from Texas Instruments). The NI USB-6221 data acquisition device serves dual purposes: monitoring the VC actuator via analog input (linear hall sensor) and VC actuation through analog output. The flow sensor interface utilizes a 32-bit microcontroller (STM32F401CCU6). An extrinsic input is introduced via a CPU exhaust fan (4715KL-04W-B40-E00), providing variable airflow with a maximum of 3.34 $m^3\,min^{-1}$ (6.87 $m\,s^{-1}$ for a rectangular duct area of $m^3 \cdot min^{-1}$; $m \cdot {}^{-1}$).

The sensor's compliant element is designed to prevent deformation due to the weight of the fin structure, ensuring minimal impact from gravity during system identification and validation experiments. The ADXL-345 accelerometer exhibited a steady-state standard deviation within ±0.008 g, while the Hall effect sensor MLX90393, used in this study, demonstrated low noise output with a steady-state standard deviation of ±5.43 μT.

The VC actuator (open-loop control) is operated by a PC running LabVIEW,[1] with its response qualitatively evaluated using a linear hall sensor. The open-loop operation of VC actuator does not ensure amplitude controlled vibration mimicking a real scenario. The linear hall sensor response is not taken into account during BVRM system identification and has limited relevance, instead the accelerometer provides the input for BVRM identification and application. The extrinsic input is generated using a CPU exhaust fan, while the VC actuator applies base vibration to the flow sensor. The VC actuator is driven by a multisine signal [see (11)] generated in LabVIEW[1] and transmitted via a National Instruments data acquisition device before reaching the custom-built audio amplifier. The microcontroller, operating in real-time operating system (RTOS) mode, captures sensor response (M_r) and accelerometer response (a_b) at 500 Hz, constrained by the sensor signal conditioning circuit. This data are crucial for BVRM identification and estimating M_b and M_s.

[1]Registered trademark.

VII. Sensor Characterization

The characteristics of whisker-inspired sensors are acquired through three stages: 1) utilizing the mathematical model; 2) conducting simulations; and 3) performing experimental tests. In line with the defined problem, simulations investigate the sensor response to both stimuli and base vibration.

A. Response From Mathematical Model

The sensor response closely resembles a second-order LTI system for base vibration as input. We investigate different base vibration magnitudes: 0.1–1.5 g. Fig. 7 shows the sensor response to base vibration input which is obtained analytically. Due to the characteristics of a second-order LTI system, the increase in the base vibration magnitude results in a proportional increase in the moment at the base.

B. Response From Simulation

To evaluate how intrinsic and extrinsic inputs affect the response of the whisker-inspired sensor, three simulations were performed as follows.

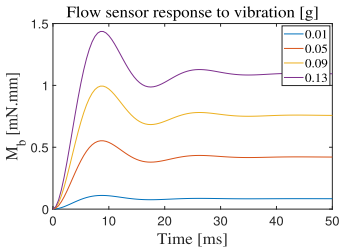

Fig. 7. Step response of the whisker sensor is presented in terms of the moment (M_b) at the base, measured in mN·mm.

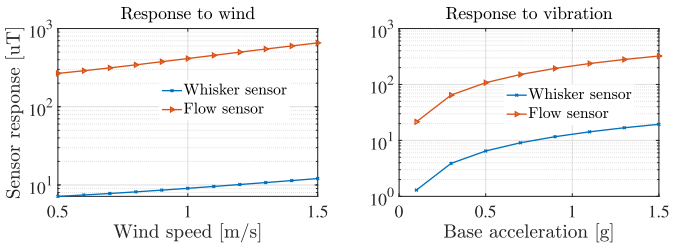

Fig. 8. Parametric response obtained from sensors in FEA study. Parametric study outputs show the steady-state response (logarithmic scale) for airflow (left) and base vibration (right).

1) The first simulation involved applying a wind load input while setting the base vibration to 0.
2) The second simulation applied a base vibration input while setting the wind load to 0.
3) The third simulation combined both base vibration and wind load inputs.

During the characterization phase, the first two simulations were examined, focusing on understanding their effects. The third simulation was specifically conducted to evaluate response separation techniques.

Fig. 8 illustrates the sensor response to a constant wind load with the base vibration set to 0 (left) and constant base vibration when the wind load is set to 0 (right). The steady-state response, with varying wind loads exhibits a nonlinear response, while the response due to varying base vibration shows a linear response. The responses are plotted in logarithmic scale to accommodate both flow and whisker sensors in one frame. Consequently, we consider the input–output relation for the transfer function g_{bb} shown in Fig. 3 as an LTI system, identified through system identification described in the next section.

C. System Identification

A multisine signal with a low crest factor is utilized for system identification in simulation, minimizing the required time while offering comprehensive insights into the frequency domain, as recommended in the literature [40]. The whisker sensor, resembling a cantilever beam, is approximated with a black box model ($\hat{G}(s)$ in (12)) of the second order or higher, as proposed in [41]. We adopt a collocated system structure where sensing and actuation occur in close proximity. Model identification employs the output error (OE) and Simplified refined instrumental variable method for continuous-time systems (SRIVC) [42]. Both methods achieve an accuracy of 91% and 87.5% for the fin sensor and whisker sensor, respectively.

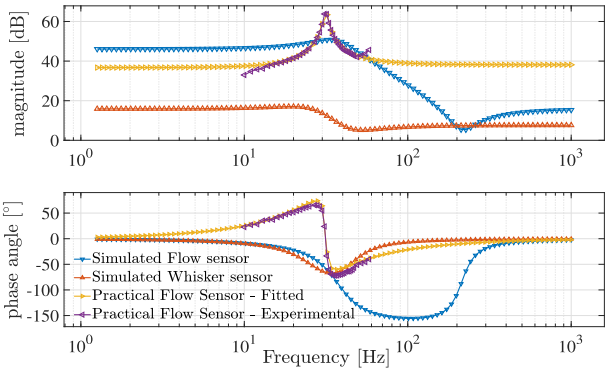

Fig. 9. Bode diagram of the simulated sensor in FEA. The 1st mode of resonance is observed at 37.32 and 27.20 Hz for simulated flow and whisker sensors, respectively, as obtained from FEA simulation. It is 31.47 Hz for the practical flow sensor shown in Fig. 6(c).

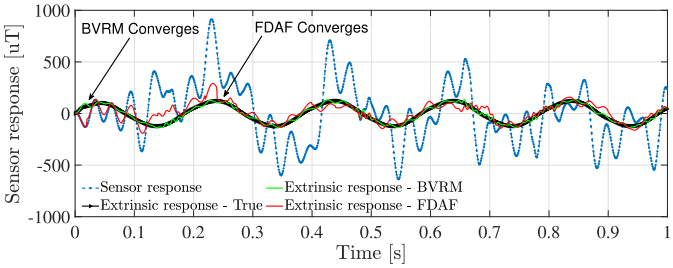

Fig. 10. Turbulent airflow and high amplitude base vibration (up to 1.5 g), where the BVRM provides the best estimation of stimulus response. FDAF converges after 0.25 s compared with the BVRM that converges quickly.

The collocated structure, typical in whiskers, generally exhibits an equal number of poles and zeros in the transfer function. The corresponding bode plot is shown in Fig. 9

$$\hat{G}(s) = \sum_{i=1}^{\infty} \frac{k_i(b_{0i}s^2 + b_{1i}s + b_{2i})}{s^2 + a_{1i}s + a_{2i}} \tag{12}$$

where k_i is the gain for ith mode.

The identification of the BVRM for the practical flow sensor utilizes the experimental setup depicted in Fig. 6(c). The identification process leverages MATLAB® and the 'TFEST' toolbox for model estimation based on the frequency-domain data [43]. The accuracy of the identified model is 94.2 %, with the 1st mode presented at 31.47 Hz, and a higher quality factor compared to the simulated model. Fig. 9 shows the corresponding bode plot and the damping ratio (ζ) for the designed sensor is found to be 0.027.

VIII. Results

A. Simulation Results

The results obtained using frequency-domain adaptive filtering (FDAF) and BVRM on sensor responses in simulation are presented in Fig. 10. With a time-varying wind load and simultaneous base vibration, the sensor response (M_r) recorded and subsequently $\hat{M}_s$ and $\hat{M}_b$ are estimated. The results illustrate the estimated $\hat{M}_s$ using FDAF and BVRM for turbulent airflow conditions and a base vibration up to 1.5 g.

The analysis of the estimated M_s shown in Fig. 10 highlights a notable difference in convergence rates between FDAF

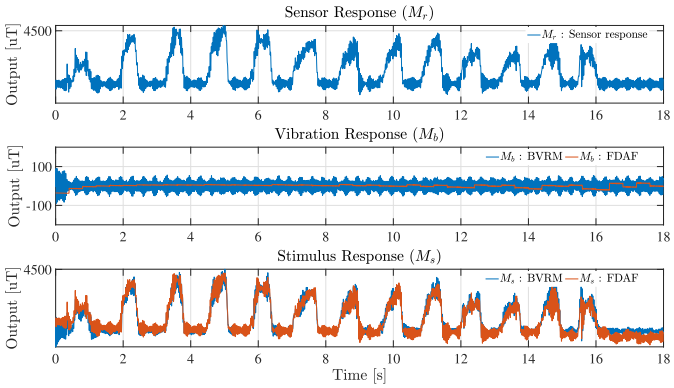

Fig. 11. Time-domain response of sensor response (M_r) given $u_s \neq 0, a_b \neq 0$ during the experiment (top). Estimated time domain response $\hat{M}_b$ from FDAF and BVRM method (middle). Estimated time domain response $\hat{M}_s$ from FDAF and BVRM method (bottom). The results shown are for base vibration up to ±0.4 g.

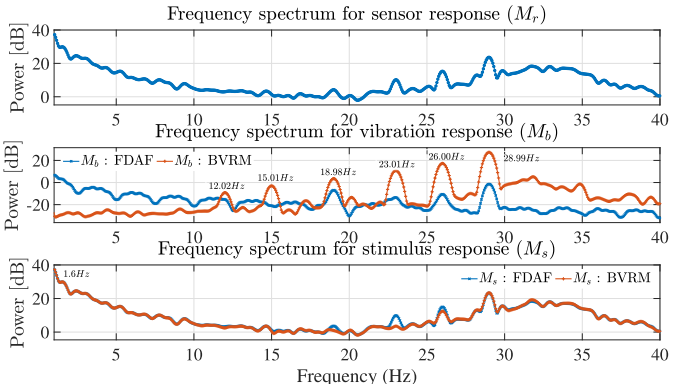

Fig. 12. Frequency response from the experiment. Frequency spectrum for M_r given $u_s \neq 0, a_b \neq 0$ (top). Frequency spectrum for the estimated base vibration response $\hat{M}_b$ from FDAF and BVRM method (middle). Frequency spectrum for $\hat{M}_s$ (bottom). The true frequencies for a_b are 12, 15, 19, 23, 26, and 29 Hz. The stimulus frequency can be qualitatively seen from Fig. 11 as ≈1.6 Hz (top).

and BVRM. Specifically, the FDAF demonstrates slower convergence, whereas BVRM displays superior performance. In particular, FDAF exhibits early divergence, whereas BVRM quickly follows the sensor response to base vibration, enabling good estimations. It is important to note that FDAF was configured with a block length of L =20 and an adaptation step size of μ =0.1. Operating in partitioned constrained mode aimed at reducing latency, FDAF demonstrated satisfactory performance, characterized by stable steady-state behavior after convergence.

B. Experimental Results

In the experimental analysis, a multisine input is employed as the base vibration. This multisine comprises frequencies that are below the first mode of the designed flow sensor, as depicted in the bode diagram in Fig. 9. Specifically, the multisine consists of frequencies in 12 Hz to 29 Hz, each with a phase shift of 30° in ascending order of frequency up to ±0.4 g. Fig. 11 illustrates the response of the flow sensor, denoted as (M_r), along with the estimated values of M_b and M_s. As shown in Fig. 8, the fin sensor is affected by both intrinsic and noncontact extrinsic inputs to a greater extent compared to the whisker sensor. Further experimentation was conducted using the designed flow sensor for additional analysis.

Fig. 11 clearly reveals the subpar performance of the FDAF even for a block length of L = 200 and an adaptation step size of μ = 0.001. Furthermore, the estimated values for M_b and M_s exhibit a deviation over time. It is crucial to note that FDAF demonstrates more reliable performance in simulations. This observation also suggests that the intrinsic and extrinsic responses in whisker-like sensors may not be purely additive in nature. Adaptive filters typically excel in scenarios with additive, coherent signals, and less dynamic interference.

To assess the effectiveness of our proposed methods in estimating M_b and M_s, we conducted a power spectrum analysis. Fig. 12 displays the power spectrum for the sensor response (M_r), followed by the sequentially estimated values of M_b and M_s. With BVRM, the estimated values for M_b and M_s accurately capture the true frequencies of the base vibration multisine. Conversely, FDAF's performance is less satisfactory, resulting in difficulties in accurately identifying these frequencies.

The power spectrums reveal FDAF's poor performance, even with an empirically set block length of 200 and an adaptation step size of 0.001 which is very slow. Both lower block lengths and higher adaptation step size resulted unstable and divergent estimations of extrinsic (airflow) and intrinsic (base vibration) responses, with noticeable drift over time (Fig. 11). Conversely, the BVRM shows robust performance, even with base vibration inputs near the first mode of vibration for the flow sensor and despite noisy accelerometer measurements. We compute the SNR considering the M_s as signal and M_b as noise. The obtained SNR with BVRM is 35.20, compared to 34.96 for the FDAF. The step size was set to 0.001 to ensure FDAF convergence which resulted in better SNR but at the cost of poor performance. The poor performance of an adaptive filter in real experiments is the nonuniform coherence between measured and reference signal [44].

C. Discussion

Decomposing M_r into M_s and M_b depends on the downstream task's requirements. Designing a universally applicable whisker-like sensor is challenging due to the influence of intrinsic input on the response to extrinsic input. Careful sensor design and simulation studies are crucial to addressing these challenges. Key observations from the study are as follows.

1) *Frequency Range:* BVRM handles a broader frequency range than adaptive filters for estimating M_s and M_b.
2) *Design Optimization:* Optimizing stiffness and damping can significantly improve sensor performance by reducing interference.
3) *Collocated Systems:* Nullifying intrinsic responses in collocated systems requires additional base actuation, increasing complexity.
4) *Reference Frame Accuracy:* Precise alignment of accelerometer reference and sensor output frames is crucial for effective separation of M_r and consideration

of the SISO technique in whisker-like sensors that are MIMO systems inherently.

5) *Data Requirements:* BVRM needs fewer reference input samples than adaptive filters, reducing computational demands.
6) *Versatility:* BVRM can be used for terrain identification without a whisker-like sensor if previously identified.
7) *Coherency in Signals:* The good coherence between sensor response and reference input is crucial for achieving effective performance with an FDAF, despite the labor-intensive nature of the filter tuning process.
8) *Sensor Design:* The design proposed in this study is simple and suitable for different types of applications, such as texture capturing fluid flow sensing, and environment exploration. Moreover, the underwater applications warrant a leak-proof design and an undulated whisker.

A comprehensive study of the proposed methods' performance across varied vibration frequencies has been conducted, with the results derived from simulations. The comparison of FDAF and BVRM performance in simulation outputs involves the consideration of metrics such as MSE, dynamic-time-warping (DTW), the difference in band power, and SNR. The response from the simulated sensor to fluid flow serves as the baseline for this evaluation. While MSE provides the cumulative error in actual and estimated, DTW provides the spatiotemporal similarity of actual and estimated sensor responses. It is observed that the BVRM outperforms FDAF, despite the simplicity of the assumed LTI model for the separation of M_r to $\hat{M}_s$ and $\hat{M}_b$.

IX. Conclusion

The FEA simulation and experimental study confirm the collocated system behavior of the whisker-like sensor. Experimental findings emphasize the effectiveness of the proposed BVRM, with a higher SNR value and robust performance, compared with the FDAF in decomposing the sensor response. Accurate estimation of M_s and M_b enhances performance in tasks, such as surface profile determination and terrain identification. The proposed BVRM enables simulation of whisker-like sensor behavior using accelerometer readings alone, eliminating the need for a physical sensor. Consistency among the mathematical model, simulation, and experimental results bolsters the validity of the approach. While tested for uniaxial readings, the methods are scalable to multiaxial implementations. The study advocates for the use of physics-based computational methods, showcasing their ability to simulate and validate whisker sensor principles with FSI. Importantly, generating multidimensional vibrations for studying sensor responses through simulation is highlighted as a more convenient task compared with the complexities of a physical experimental setup.

Some of the limitations of this study are the following. It considers low base vibration amplitudes (up to 1.5 g) and moderate wind speeds (up to 4 $\mathrm{m\,s^{-1}}$), while the whisker sensor is sensitive to higher amplitudes. The deterministic model for decomposing sensor response may not universally apply due to varying sensor structures and material properties. Although the linear model fits well in simulation and experiments, a nonlinear BVRM could enhance performance. The sensor design lacks optimization for controlled damping and stiffness, which could improve response separation. While some tasks may require an active whisker sensor, this study employs a passive arrangement. Finally, the proposed BVRM method is adaptable and reconfigurable based on downstream task requirements and MIMO system analysis methods.

References

[1] C. W. S. To, "Vibration of a cantilever beam with a base excitation and tip mass," *J. Sound Vib.*, vol. 83, no. 4, pp. 445–460, Aug. 1982.
[2] J. H. Williams Jr., *Fundamentals of Applied Dynamics*. Cambridge, MA, USA: MIT Press, 2019.
[3] A. E. T. Yang and M. J. Z. Hartmann, "Whisking kinematics enables object localization in head-centered coordinates based on tactile information from a single vibrissa," *Frontiers Behav. Neurosci.*, vol. 10, p. 145, Jul. 2016.
[4] M. J. Hartmann, N. J. Johnson, R. B. Towal, and C. Assad, "Mechanical characteristics of rat vibrissae: Resonant frequencies and damping in isolated whiskers and in the awake behaving animal," *J. Neurosci.*, vol. 23, no. 16, pp. 6510–6519, Jul. 2003.
[5] R. A. Russell, "Closing the sensor-computer-robot control loop," *Robot. Age*, vol. 6, no. 4, pp. 15–20, 1984.
[6] E. L. Starostin, V. G. A. Goss, and G. H. M. van der Heijden, "Whisker sensing by force and moment measurements at the whisker base," *Soft Robot.*, vol. 10, no. 2, pp. 326–335, Apr. 2023.
[7] M. J. Pearson, A. G. Pipe, C. Melhuish, B. Mitchinson, and T. J. Prescott, "Whiskerbot: A robotic active touch system modeled on the rat whisker sensory system," *Adapt. Behav.*, vol. 15, no. 3, pp. 223–240, Sep. 2007.
[8] R. A. Russell and J. A. Wijaya, "Object location and recognition using whisker sensors," in *Proc. Australas. Conf. Robot. Automat.*, 2003, pp. 761–768.
[9] A. Tagliabue and J. P. How, "Airflow-inertial odometry for resilient state estimation on multirotors," in *Proc. IEEE Int. Conf. Robot. Autom. (ICRA)*, May 2021, pp. 5736–5743.
[10] T. Wang, T. A. Kent, and S. Bergbreiter, "Design of whisker-inspired sensors for multi-directional hydrodynamic sensing," 2023, *arXiv:2307.09569*.
[11] S. Kim, R. Kubicek, A. Paris, A. Tagliabue, J. P. How, and S. Bergbreiter, "A whisker-inspired fin sensor for multi-directional airflow sensing," in *Proc. IEEE/RSJ Int. Conf. Intell. Robots Syst. (IROS)*, Oct. 2020, pp. 1330–1337.
[12] C. Barbier, J. A. Humphrey, J. Paulus, and M. Appleby, "Design, fabrication and testing of a bioinspired hybrid hair-like fluid motion sensor array," in *Proc. ASME Int. Mech. Eng. Congr. Expo.*, vol. 43025, 2007, pp. 1319–1324.
[13] J. B. Stocking, W. C. Eberhardt, Y. A. Shakhsheer, B. H. Calhoun, J. R. Paulus, and M. Appleby, "A capacitance-based whisker-like artificial sensor for fluid motion sensing," in *Proc. IEEE SENSORS*, Nov. 2010, pp. 2224–2229.
[14] W. C. Eberhardt, Y. A. Shakhsheer, B. H. Calhoun, J. R. Paulus, and M. Appleby, "A bio-inspired artificial whisker for fluid motion sensing with increased sensitivity and reliability," in *Proc. IEEE SENSORS*, Oct. 2011, pp. 982–985.
[15] J. P. Wissman, K. Sampath, S. E. Freeman, and C. A. Rohde, "Capacitive bio-inspired flow sensing cupula," *Sensors*, vol. 19, no. 11, p. 2639, Jun. 2019.
[16] N. F. Lepora, M. Pearson, and L. Cramphorn, "TacWhiskers: Biomimetic optical tactile whiskered robots," in *Proc. IEEE/RSJ Int. Conf. Intell. Robots Syst. (IROS)*, Oct. 2018, pp. 7628–7634.
[17] T. A. Kent, S. Kim, G. Kornilowicz, W. Yuan, M. J. Z. Hartmann, and S. Bergbreiter, "WhiskSight: A reconfigurable, vision-based, optical whisker sensing array for simultaneous contact, airflow, and inertia stimulus detection," *IEEE Robot. Autom. Lett.*, vol. 6, no. 2, pp. 3357–3364, Apr. 2021.
[18] S. R. Anderson, M. J. Pearson, A. Pipe, T. Prescott, P. Dean, and J. Porrill, "Adaptive cancelation of self-generated sensory signals in a whisking robot," *IEEE Trans. Robot.*, vol. 26, no. 6, pp. 1065–1076, Dec. 2010.
[19] A. Tagliabue, A. Paris, S. Kim, R. Kubicek, S. Bergbreiter, and J. P. How, "Touch the wind: Simultaneous airflow, drag and interaction sensing on a multirotor," in *Proc. IEEE/RSJ Int. Conf. Intell. Robots Syst. (IROS)*, Oct./Jan. 2021, pp. 1645–1652.
[20] Z. Yu, S. Perera, H. Hauser, P. R. N. Childs, and T. Nanayakkara, "A tapered whisker-based physical reservoir computing system for mobile robot terrain identification in unstructured environments," *IEEE Robot. Autom. Lett.*, vol. 7, no. 2, pp. 3608–3615, Apr. 2022.

[21] C. Brooks, K. Iagnemma, and S. Dubowsky, "Vibration-based terrain analysis for mobile robots," in *Proc. IEEE Int. Conf. Robot. Autom.*, Apr. 2005, pp. 3415–3420.
[22] W. Deer and P. E. I. Pounds, "Lightweight whiskers for contact, pre-contact, and fluid velocity sensing," *IEEE Robot. Autom. Lett.*, vol. 4, no. 2, pp. 1978–1984, Apr. 2019.
[23] J. H. Solomon and M. J. Z. Hartmann, "Extracting object contours with the sweep of a robotic whisker using torque information," *Int. J. Robot. Res.*, vol. 29, no. 9, pp. 1233–1245, Aug. 2010.
[24] P. K. Routray, A. S. Kanade, K. Tiwari, P. Pounds, and M. Muniyandi, "Towards multidimensional textural perception and classification through whisker," in *Proc. IEEE Int. Symp. Robotic Sensors Environments (ROSE)*, Nov. 2022, pp. 1–7.
[25] J. Z. Gul, K. Y. Su, and K. H. Choi, "Fully 3D printed multi-material soft bio-inspired whisker sensor for underwater-induced vortex detection," *Soft Robot.*, vol. 5, no. 2, pp. 122–132, Apr. 2018.
[26] A. M. Kamat, X. Zheng, J. Bos, M. Cao, M. S. Triantafyllou, and A. G. P. Kottapalli, "Undulating seal whiskers evolved optimal wavelength-to-diameter ratio for efficient reduction in vortex-induced vibrations," *Adv. Sci.*, vol. 11, no. 2, Jan. 2024, Art. no. 2304304.
[27] S. Skogestad and I. Postlethwaite, *Multivariable Feedback Control: Analysis and Design*. Hoboken, NJ, USA: Wiley, 2005.
[28] M. A. Lin, E. Reyes, J. Bohg, and M. R. Cutkosky, "Whisker-inspired tactile sensing for contact localization on robot manipulators," in *Proc. IEEE/RSJ Int. Conf. Intell. Robots Syst. (IROS)*, Oct. 2022, pp. 7817–7824.
[29] S. S. Haykin, *Adaptive Filter Theory*. London, U.K.: Pearson, 2002.
[30] J. Chen, J. Benesty, Y. Huang, and S. Doclo, "New insights into the noise reduction Wiener filter," *IEEE Trans. Audio, Speech, Lang., Process.*, vol. 14, no. 4, pp. 1218–1234, Jul. 2006.
[31] J. A. Anderson and E. Rosenfeld, Eds., *Neurocomputing: Foundations of Research*, vol. 1. Cambridge, MA, USA: MIT Press, 1988, pp. 123–134, doi: 10.7551/mitpress/4943.001.0001.
[32] K. K. Leang and S. Devasia, "Feedback-linearized inverse feedforward for creep, hysteresis, and vibration compensation in AFM piezoactuators," *IEEE Trans. Control Syst. Technol.*, vol. 15, no. 5, pp. 927–935, Sep. 2007.
[33] D. Croft, G. Shed, and S. Devasia, "Creep, hysteresis, and vibration compensation for piezoactuators: Atomic force microscopy application," *J. Dyn. Syst., Meas., Control*, vol. 123, no. 1, pp. 35–43, Mar. 2001.
[34] T. R. Kane, R. Ryan, and A. Banerjeer, "Dynamics of a cantilever beam attached to a moving base," *J. Guid., Control, Dyn.*, vol. 10, no. 2, pp. 139–151, 1987.
[35] S. Kim, C. Velez, D. K. Patel, and S. Bergbreiter, "A magnetically transduced whisker for angular displacement and moment sensing," in *Proc. IEEE/RSJ Int. Conf. Intell. Robots Syst. (IROS)*, Nov. 2019, pp. 665–671.
[36] O. H. Yeoh, "Some forms of the strain energy function for rubber," *Rubber Chem. Technol.*, vol. 66, no. 5, pp. 754–771, Nov. 1993.
[37] K. Sisanth, M. Thomas, J. Abraham, and S. Thomas, "General introduction to rubber compounding," in *Progress in Rubber Nanocomposites*. Amsterdam, The Netherlands: Elsevier, 2017, pp. 1–39.
[38] S. Pan, Q. C. Nguyen, V. T. Nguyen, and J. S. Welsh, "Continuous-time system identification of a flexible cantilever beam," in *Proc. IEEE Conf. Control Technol. Appl. (CCTA)*, 2021, pp. 868–873.
[39] C. Weiss, H. Frohlich, and A. Zell, "Vibration-based terrain classification using support vector machines," in *Proc. IEEE/RSJ Int. Conf. Intell. Robots Syst.*, Oct. 2006, pp. 4429–4434.
[40] D. Rees, D. L. Jones, and D. C. Evans, "Practical considerations in the design of multisine test signals for system identification," in *Proc. Conf. Rec. IEEE Instrum. Meas. Technol. Conf.*, May 1992, pp. 174–179.
[41] V. Sethi and G. Song, "Multimodal vibration control of a flexible structure using piezoceramic sensor and actuator," *J. Intell. Mater. Syst. Struct.*, vol. 19, no. 5, pp. 573–582, 2008.
[42] A. Padilla, H. Garnier, and M. Gilson, "Version 7.0 of the CONTSID toolbox," *IFAC-PapersOnLine*, vol. 48, no. 28, pp. 757–762, 2015.
[43] H. Lei, C. Lim, and X. Tan, "Modeling and inverse compensation of dynamics of base-excited ionic polymer–metal composite sensors," *J. Intell. Mater. Syst. Struct.*, vol. 24, no. 13, pp. 1557–1571, Sep. 2013.
[44] A. Grinsted, J. C. Moore, and S. Jevrejeva, "Application of the cross wavelet transform and wavelet coherence to geophysical time series," *Nonlinear Processes Geophys.*, vol. 11, nos. 5–6, pp. 561–566, Nov. 2004.